ARTICLE

Corrugation of Chemically Converted Graphene Monolayers on SiO_2

Alexander Sinitskii, Dmitry V. Kosynkin, Ayrat Dimiev, and James M. Tour*

Departments of Chemistry, Computer Science, Mechanical Engineering and Materials Science, and the Smalley Institute for Nanoscale Science and Technology, Rice University, MS 222, 6100 Main Street, Houston, Texas 77005

ABSTRACT Sheets of chemically converted graphene (CCG) on the surface of Si/SiO_2 substrates exhibit nanoscopic corrugation. This corrugation has been assumed to be caused by a combination of factors including (a) thermal treatments in the device preparation, (b) different oxygen-containing addends on the CCG, and (c) the substrate roughness. In this paper, we study the interplay of these factors in the corrugation behavior of monolayer CCG flakes, prepared by reduction of graphene oxide (GO) synthesized by Hummers method, and CCG nanoribbons, produced by chemical unzipping of carbon nanotubes, followed by the reduction by hydrazine at 95 °C. We have studied the morphology, composition, and electrical properties of the flakes and nanoribbons before and after annealing in Ar/H_2 at 300 °C. Our experiments demonstrate that, despite the temperature treatment and the associated removal of the oxygen-containing addends from the basal plane of the CCG, the corrugation pattern of the CCG exhibits almost no change upon annealing. This suggests that the substrate roughness, not the chemical addends nor the thermal cycling, is the predominant determinant in the graphene corrugation. This conclusion is supported by depositing GO flakes on freshly cleaved mica. Such flakes were shown to have extremely low corrugation (rms ∼70 pm), as dictated by the atomically flat surface of mica. Our experimental observations are in accord with the results of our molecular dynamics simulations, which show that interaction with the substrate greatly suppresses the intrinsic corrugation of graphene materials.

KEYWORDS: graphene · graphene oxide · corrugation · chemical functionalization · unzipping of carbon nanotubes · atomic force microscopy

Graphene is a two-dimensional material composed of carbon atoms packed in a honeycomb lattice.[1] Graphene is attracting enormous interest due to its remarkable electronic, mechanical, and thermal properties.[2−4] Interestingly, a decades-long question regarding graphene was whether it could even exist because it was believed that two-dimensional crystals are not stable at any finite temperature.[5,6] One of the reasons for the stability of free-standing graphene could be its observed wrinkling into the third dimension.[7−9] This intrinsic rippling of suspended graphene membranes was theoretically shown to be caused by thermal fluctuations.[10] Of recent practical importance is graphene behavior when atop a SiO_2 substrate because this is the most common embodiment for electronic devices made from this material. In addition to the intrinsic corrugation, graphene sheets deposited on a SiO_2 surface also exhibit inevitable wrinkling due to the roughness of the substrate.[11,12] Understanding the interplay between the different factors affecting the corrugation of graphene is an issue of practical importance[13] as the wrinkling is thought to be one of the major factors limiting its electronic mobility.[14,15]

Corrugation should also be observed for chemically converted graphene (CCG), which is produced by reduction of graphene oxide (GO).[16−21] However, with CCG, the conditions leading to corrugation are more complex because the intrinsic corrugation could be caused by various nonregular oxygen-containing addends that are present on the edges and basal planes of the CCG.[16,17] Simulations suggest that different addends and their arrangements may result in significant wrinkling and even bending of graphene sheets.[17,22] However, the interplay of the different factors affecting the corrugation of CCG has not been experimentally studied. In this paper, we report the theoretical and experimental study of the corrugation of CCG on the Si/SiO_2 substrate and show that the corrugation is almost entirely substrate-dependent.

Previous theoretical work suggested that different functional addends, vacancies, topological defects,[17,22] and adsorbed molecules[23] greatly enhance the corrugation of graphene sheets. However, all of these previous simulations have been carried out for free-standing graphene or GO in vacuum, and the results therefore can only be comfortably applied to the explanation of the corrugation behavior of suspended sheets.[24] Previous simulations have not considered the interaction of graphene sheets

*Address correspondence to tour@rice.edu.

Received for review February 15, 2010 and accepted April 28, 2010.

Published online May 6, 2010.
10.1021/nn100306r

© 2010 American Chemical Society

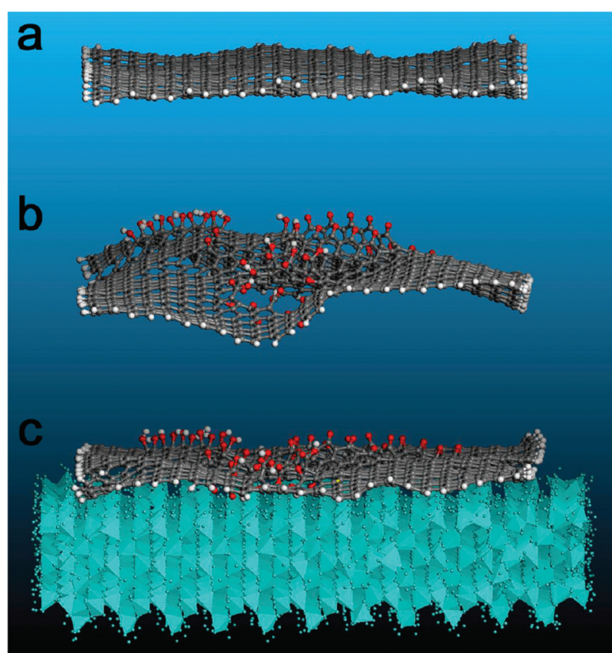

Figure 1. Simulated corrugation of (a) free-standing graphene, (b) free-standing GO, and (c) GO on the surface of hydroxyl-terminated (111) quartz.

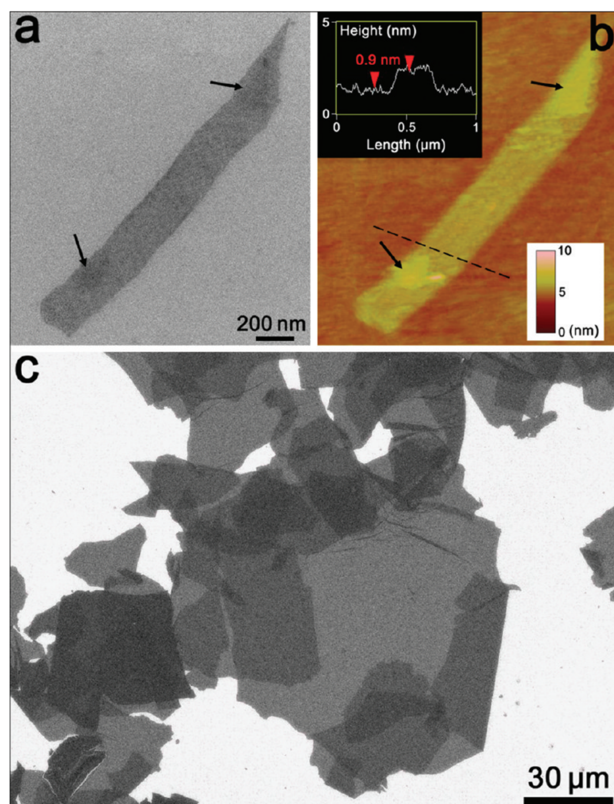

Figure 2. CCG materials used in this work. (a) SEM and (b) AFM images of the same monolayer GNR after reduction by hydrazine. The top inset in (b) shows a height profile along the dashed line. The arrows in (a) and (b) show the small pieces of another monolayer GNR, which effectively form bilayer regions. (c) SEM image of the large CCG flakes prepared by hydrazine reduction of GO synthesized by the Hummers method.

with the substrate and its influence on the corrugation of graphene. Here we demonstrate that such surface interactions play the dominant role in the corrugation of graphene.

Figure 1a shows a graphene sheet (N_C = 1032) terminated with the hydrogen atoms (N_H = 90) and suspended in vacuum. This sheet exhibits slight corrugation, which has been previously experimentally found for suspended graphene.[7−9] The observed ripples are <0.5 nm high and 5−20 nm wide, which is in accord with the experimental data.[7−9] The same graphene sheet was then used to construct the model of GO: a row of epoxy groups (N_O = 5) was added, one isolated epoxy moiety, a row of vicinal hydroxyl groups (N_O = 10), one isolated pair of vicinal hydroxyl groups (N_{OH} = 2), a row of paired carbonyl groups (N_{CO} = 10), an isolated pair of paired carbonyl groups, and a hole surrounded with six carboxyl groups (N_{COOH} = 6) and four carbonyls (N_{CO} = 4) on the basal plane. Figure 1b shows that, indeed, GO has severely enhanced corrugation with an increased amplitude of the ripples in comparison to graphene. However, such corrugation might be observed for suspended GO only.[24] In the following simulations, we put the same GO sheet upon the surface of a hydroxyl-terminated slab of (111) quartz, which we have employed as a proxy for amorphous silicon dioxide, the latter of which covers silicon wafers as typical substrates for graphene/GO electronic devices. Figure 1c shows that, once in contact with the substrate, the vacuum-corrugated GO sheet flattens and the amplitude of corrugation becomes comparable to that of free-standing graphene (Figure 1a).

For the experimental part of this study, we used the GO nanoribbons (GONRs) obtained by the oxidative unzipping of multiwalled carbon nanotubes (MWCNTs) in a sulfuric acid solution of potassium permanganate, as reported in our previous work,[25] and also GO flakes obtained by a conventional Hummers method.[26]

Before deposition on Si/SiO_2 substrates, the GO flakes and GONRs were reduced by hydrazine at 95 °C to chemically converted graphene (CCG) flakes and graphene nanoribbons (GNRs), respectively. This treatment partially reduces the GO but still leaves many of the surface groups unaltered. The reduced materials were then dispersed over the Si/SiO_2 substrates (heavily doped p-type Si with 200 nm thick thermal SiO_2 layer; SQI).[27] Figure 2 shows the images of both types of CCG materials on Si/SiO_2, obtained by scanning electron microscopy (SEM) and atomic force microscopy (AFM).

Among different GNRs and CCG flakes on the substrates, only the single-layer flakes were selected by SEM and AFM and then used for the fabrication of the electronic devices (Figure 3).[27−29] The schematic of a typical device is shown in Figure 3a.[30,31] Figure 3b shows

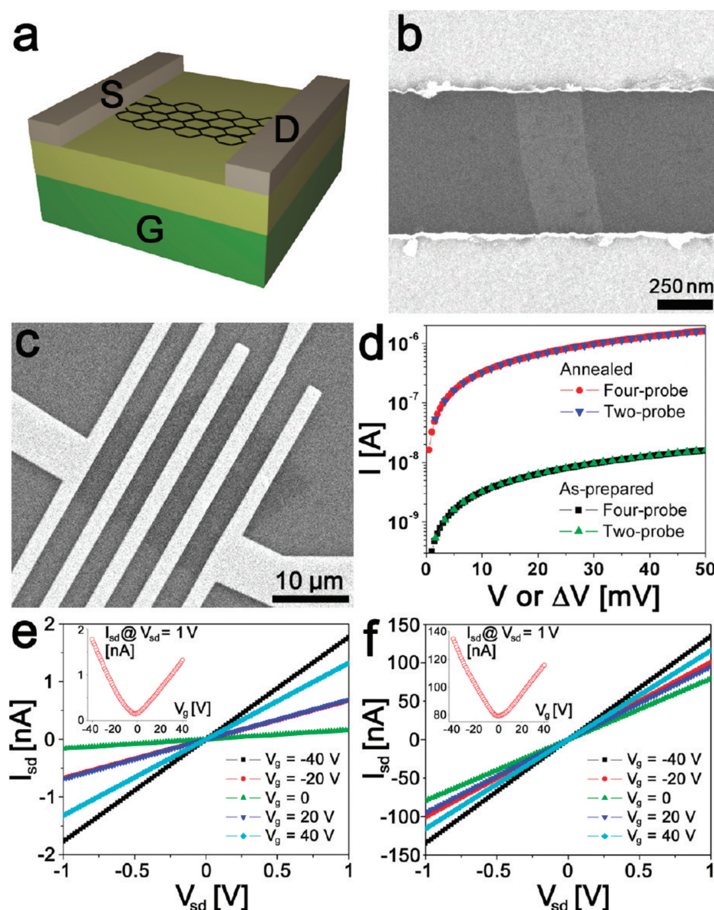

Figure 3. Electronic devices based on GNRs and CCG. (a) Schematic of a device; 20 nm thick e-beam deposited Pt metal serves as the source (S) and drain (D) electrodes. The device is fabricated on a 200 nm thick thermal SiO_2 over heavily doped p-type Si that is used as a back gate (G). (b) Top-view SEM image of a typical electronic device based on a single-layer GNR. (c) SEM image of a typical multi-terminal electronic device based on a single-layer CCG flake. (d) Current−voltage (*IV*) dependencies for the same electronic device based on a single-layer CCG before and after annealing in H_2/Ar at 300 °C for 30 min measured by both two- and four-probe methods. (e,f) Source−drain current (I_{SD}), source−drain voltage (V_{sd}), and gate voltage (V_g) dependencies (p-doped silicon was used as a back gate) for the same device based on a hydrazine-reduced monolayer GNR (e) before and (f) after annealing in H_2/Ar at 300 °C for 30 min.

the SEM image of a typical electronic device based on a single-layer GNR used for this study. Overall, 14 devices were fabricated and studied; the widths of GNRs were 200−300 nm and the electrode spacings were 600−800 nm. Out of 14 GNRs used for the device fabrication, two were long enough to fabricate four-terminal devices. In contrast, monolayer CCG flakes found on Si/SiO_2 substrates were large enough to fabricate multi-terminal electronic devices, as shown in Figure 3c.

We also prepared samples with uniform thick (>1 μm) coatings of densely packed GNRs for the X-ray photoelectron spectroscopy (XPS) studies; these samples were fabricated by casting concentrated solutions of GNRs onto the Si/SiO_2 substrates and evaporating the solvent. Similar CCG flake samples for the XPS analysis were also prepared. The electronic devices and thick films were subjected to the same reduction conditions (annealing in Ar/H_2 at 300 °C for 30 min), and AFM, *IV*, and XPS data were collected for both hydrazine-reduced and further annealed samples.

XPS and *IV* data suggest that annealing results in significant changes in the chemical composition and structure of CCG. The C1s XPS spectra show the decrease in the amount of oxygen-containing functionalities in the GONRs upon reduction (Figure 4). The peak at 284.8 eV corresponds to C−C bonds, whereas the overlapping peaks at 286−289 eV correspond to the carbon in different oxygen-containing functional groups. As expected, these peaks are still seen after the reduction with hydrazine, though their intensity decreased dramatically in comparison to the starting GONRs. After annealing the reduced nanoribbons in Ar/H_2 at 300 °C for 30 min, the peak at 286.8 eV (C−O bonds) diminishes, and only a small shoulder at 288.8 eV is still observed, which probably corresponds to the edge and hole-edge carboxylic acid moieties. Similar XPS results were obtained for the large flakes.

The removal of oxygen-containing functionalities results in an increased number of sp^2 carbons in the GNR, which in turn dramatically affects its conductivity. This effect is illustrated by Figure 3, which displays the electrical properties for the same device based on a hydrazine-reduced monolayer ribbon before (Figure 3e) and after (Figure 3f) annealing in H_2/Ar at 300 °C for 30 min. The electrical properties of the annealed device were qualitatively the same though its conductivity at zero gate

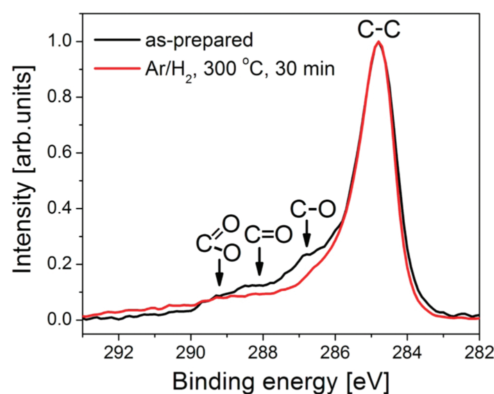

Figure 4. C1s XPS spectra for GNRs with different degrees of reduction (as-prepared are hydrazine-reduced) showing that annealing removes significant residual oxygenated content from the nanoribbons.

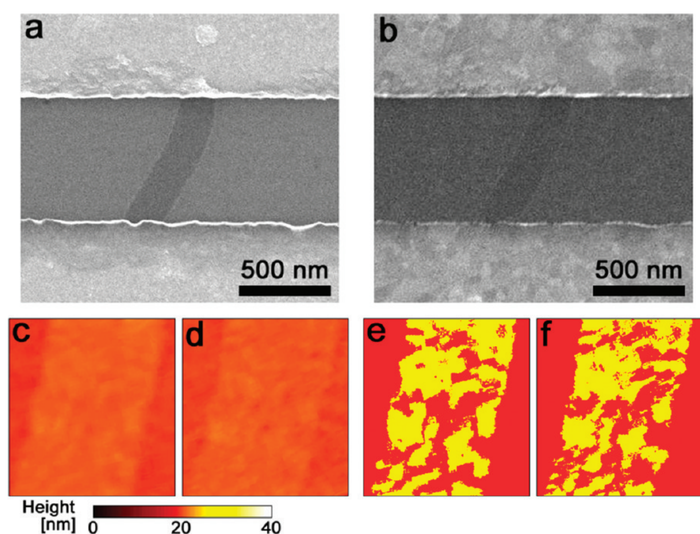

Figure 5. Effect of annealing on the appearance of GNRs. SEM images of the same electronic device based on a single-layer GNR (a) before and (b) after annealing. Using the same GNR as in (a) and (b), two 364 × 388 nm^2 AFM images of the portion are shown (c) before and (d) after annealing at 300 °C. (e,f) Results of processing of the images from (c) and (d), respectively (see text for details) to highlight the peaks (yellow) and the valleys (red).

bias increased 500-fold after annealing. Noteworthy, both preannealed and annealed devices exhibited ambipolar electrical field effects typical of graphene (see the insets in Figure 3e,f).[1−3] Similar results were obtained for multiterminal GNR devices annealed in H_2/Ar at 300 °C for 30 min and measured by the four-probe method; they exhibited a 2 orders of magnitude increase in conductivity on average. Devices based on CCG flakes behave the same way. Figure 3d shows *IV* data for the same electronic device based on a CCG flake recorded before and after annealing in H_2/Ar at 300 °C by both two- and four-probe methods. The conductivity of these flakes also increased by about 2 orders of magnitude upon annealing (8 devices were tested). Remarkably, there is almost no difference between the *IV* curves measured by two- and four-terminal methods, suggesting that the contribution of the contact resistance to the total device resistance is negligible relative to the impact of the resistance of the CCG flake.

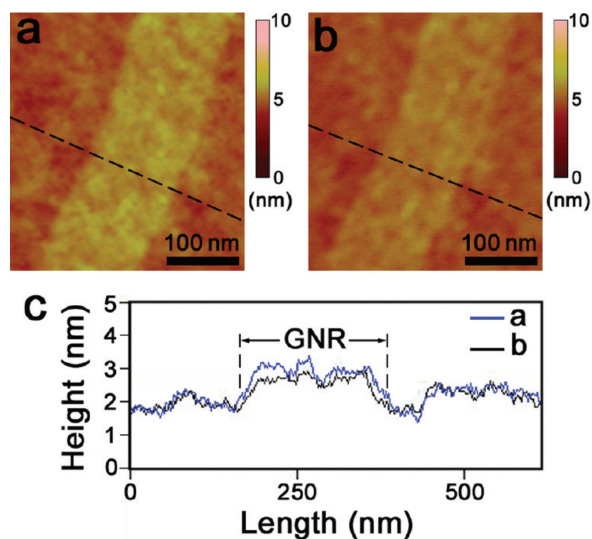

Figure 6. AFM images of the same GNR measured before (a) and after (b) annealing in H_2/Ar at 300 °C along with the corresponding height profiles (c). The height profiles were measured along the same dashed line, shown both in (a) and (b). Note that the height profiles of the Si/SiO_2 substrate before and after annealing nearly perfectly match each other. This GNR was never treated with any resist.

Recent experiments performed on graphene membranes suspended over the trench in the Si/SiO_2 substrate demonstrate that, upon annealing to 125−330 °C and subsequent cooling to room temperature, the corrugation of the sheet changes dramatically.[32] This effect is attributed to the fact that graphene has a negative thermal expansion coefficient (TEC). While at high temperatures the silicon substrate expands, the graphene sheet, in contrast, shrinks, thus pulling graphene in the trench area. However, after cooling to room temperature, the excessive graphene in the trench results in the formation of large wrinkles in the membrane.[32] One could expect that the large difference in the TECs of the Si/SiO_2 substrate and the CCG would also result in a dramatic change in the corrugation of the latter after annealing. Furthermore, the removal of the oxygen-containing functional groups from the basal plane of monolayer CCG flake or ribbon upon annealing could also contribute to the change in its corrugation pattern.

On the contrary, our experiments demonstrate that, despite the above factors, the corrugation pattern of the CCG ribbons exhibits almost no change upon annealing. Figure 5a,b shows SEM images of the same two-terminal device based on a hydrazine-reduced monolayer ribbon before and after annealing, respectively. The appearance of the electrodes changes due to the crystallization of Pt. Figures 5c and d show AFM images of the middle portion of the same electronic device before and after annealing, respectively. In both AFM images, the GNR exhibits nanoscopic corrugation, where 20−30 nm sized valleys are separated by wrinkles. Importantly, the nearby Si/SiO_2 exhibited similar peak-and-valley topography. The length scales of the GNR corrugation and the substrate roughness were the same, ∼20−30 nm. For all GNRs studied in this work, it has been found that the substrate and the ribbon have similar roughness (rms ∼0.23−0.25 nm) as measured for different areas of substrate and GNRs both before and after annealing. These experimental observations suggest that (1) the roughness of the substrate affects the corrugation of nanoribbons, and (2) the corrugation of GNRs does not dramatically change upon annealing. To further verify this conclusion, we compared the corrugation patterns for the same GNR before and after annealing. The darker regions, corresponding to the valleys, occupy the same parts of the ribbon before and after annealing, suggesting that

these darker regions are not artifacts of the measurements, and once formed, the nanoscopic structure of the ribbon is stable even upon temperature treatment. To illustrate this effect, we have processed the AFM images in Figure 5c,d in such a way that we used a threshold height (h_{th}) and thereby characterize the regions of the GNR with $h > h_{th}$ (peaks) and $h < h_{th}$ (valleys) by two different colors: yellow and red, correspondingly. The results of this processing upon Figure 5c,d are shown in Figure 5e,f, respectively, which demonstrate that the corrugation pattern of the GNR does not significantly change after annealing at 300 °C. The peaks remained as peaks and the valleys as valleys, suggesting that neither the loss of covalently bonded surface addends nor the TEC are responsible for the corrugation. The starting SiO_2 surface roughness dominates the corrugation of the graphene. The shape of some valleys slightly changed, though this could be attributed to the inaccuracy of the "threshold height" analysis, which is vulnerable in the intermediate regions between peaks and valleys. Most importantly, no existing valley disappeared, no new valley appeared, and the relative position of the valleys did not change after annealing. The corrugation pattern remained predominantly intact.

Previously, it was pointed out that graphene flakes subjected to the device fabrication process could be contaminated by resist residues, unless annealed in Ar/H_2.[11] Therefore, although the device results discussed so far were conveniently obtained as the *IV* and morphology data could be collected for the same GNR, it could be argued that the ribbons before and after annealing in Ar/H_2 were different in that unannealed ribbons bear PMMA residues in spite of the extensive acetone washings. Despite the possible presence of such contamination, the ribbons still exhibit the same peak-and-valley patterns before and after annealing, suggesting that PMMA residues might affect the apparent height of the ribbons rather than their peak-and-valley patterns. Hence, to avoid possible ambiguities, we also performed the same AFM experiment before and after annealing in H_2/Ar at 300 °C on the GNRs on separate Si/SiO_2 substrates that were not used for the device fabrication and thus never treated with any resist. Typical results of such AFM analyses are shown in Figure 6. The peak-and-valley pattern of this GNR does not change upon annealing, which is in accord with the previously discussed data. This can be seen by comparing not only Figure 6a,b but also the corresponding height profiles. Figure 6c shows a typical set of two height profiles of the same GNR measured along the same line before and after annealing in H_2/Ar at 300 °C. The morphologies of both the GNR and Si/SiO_2 substrate remain the same after the thermal treatment. Interestingly, in such height profiles, the GNRs consistently appear to be slightly thinner after annealing by 0.1−0.2 nm. After 40 min of hydrazine reduction, the monolayer ribbons typically had a thickness of 0.7−1.1 nm, which is in a good agreement with the reported thickness of reduced GO.[18−21] After reduction of the GNRs in H_2/Ar at 300 °C, the thicknesses at different points of the previously measured ribbons decreased to 0.5−0.9 nm. The observed structural transformation of GNRs could be partially associated with the removal of some oxygen-containing functional groups from the surface of the nanoribbons, which was previously observed by XPS. It may also be caused by the annealing-induced removal of the traces of different species (such as water, hydrazine, atmospheric gases) that could be trapped between the ribbon or CCG flake and Si/SiO_2, as the CCG materials were deposited on the substrates from aqueous solutions of hydrazine. The contraction−expansion process[32] discussed above might also have an impact on the apparent height of the ribbon upon annealing, so that the GNR might better conform to the substrate after the thermal treatment.

Interestingly, Geringer *et al.* have reported on corrugation of mechanically exfoliated graphene: while the corrugation of SiO_2 is long-range with a correlation length of about 25 nm, some of the graphene monolayers exhibited an additional corrugation with a preferential wavelength of about 15 nm.[13] In contrast, Ishigami *et al.* have shown that graphene on Si/SiO_2 has a larger correlation length than the substrate (32 *versus* 23 nm, respectively) and a smaller height variation (1.9 *versus* 3.1 Å, respectively), suggesting that graphene is "flatter" than the substrate.[11] In our work, we did not observe such short-range corrugation, neither by SEM (as we discuss below) nor by AFM. Furthermore, it is probable that such intrinsic corrugation would have been affected by annealing, whereas in our case, no change in the corrugation pattern was observed upon annealing. These results suggest that the morphology of graphene materials on different substrates may be preparation-dependent. It is possible that different methods of depositing the graphene on the substrate, such as from a solution or by a "drawing", may also be important in differentiating the source of the corrugation. In particular, we anticipate that CCG flakes deposited from solution, as in our case, may conform to the substrate better than the flakes deposited by a dry technique, although this obviously requires further experimental verification. We also note that the interface between the hydrophilic GO flakes and SiO_2 should be more energetically favorable than that between the hydrophobic graphene and SiO_2.

One of the important practical conclusions that could be made from this work is that extremely flat, previously inaccessible flakes of graphene and GO could be achieved if placed on top of an atomically flat substrate because intrinsic ripples and the corrugation induced by different functional groups can be strongly suppressed by the interfacial van der Waals interactions of graphene with the substrate. To demonstrate this effect, we have deposited GO flakes on substrates with

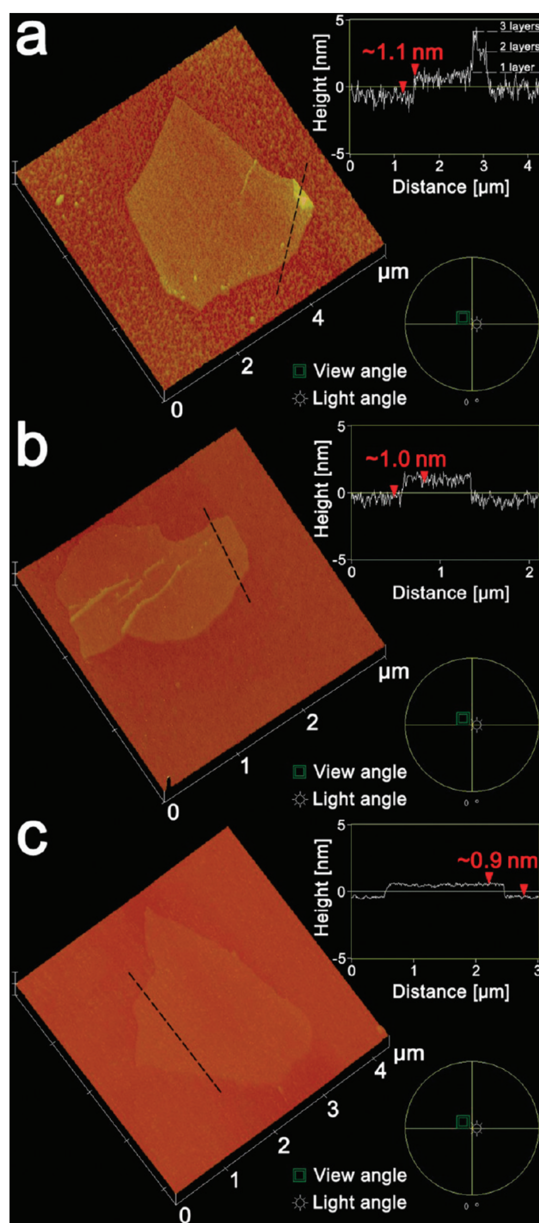

Figure 7. AFM images of monolayer GO flakes on different substrates: (a) rough SiO_2, (b) smoother SiO_2, and (c) mica. The top inset in each panel shows a height profile along the corresponding dashed line. The dashed line in (a) is intentionally drawn through the small self-folded area of the flake in order to demonstrate the steps corresponding to effective 1, 2, and 3 layers in the height profile. The bottom insets demonstrate that all three images are rotated and illuminated in the same way.

different roughnesses: "rough" Si/SiO_2 (chemically etched substrate; rms ~0.5 nm), smoother Si/SiO_2 (rms ~0.3 nm), and freshly cleaved mica. The flakes were deposited on the substrates from a dilute water solution. We note that when depositing GO on mica it is important to place a small droplet of the solution in the middle of the substrate because a large amount of water, especially if close to the edge, degrades the surface. Figure 7 shows AFM images of GO flakes on the above three substrates. We note that all three images have the same height scale (10 nm); they are rotated and illuminated in the same way. All flakes are monolayers and have a thickness of about 1 nm, as confirmed by the corresponding height profiles. Such images clearly show that the corrugation of GO flakes strongly correlates with the roughness of the substrate. The average roughness of the flakes on the "rough" Si/SiO_2 was rms ~0.38 nm, on the smoother Si/SiO_2 the rms ~0.3 nm, and for the flakes on mica, we have measured extremely low rms ~0.07 nm. This indicates that the substrate roughness is a key factor in the corrugation of graphene materials, whereas other factors have smaller impact. Interestingly, in the case of the GO flakes on mica and Si/SiO_2, we have measured almost the same roughness characteristics for both the flakes and the substrates. However, on the rough Si/SiO_2, the GO flake is smoother than the substrate (rms ~0.38 *versus* ~0.5 nm). This suggests that, for the rough substrates that are not typically used for graphene materials, the flake may not perfectly conform to the surface of the substrate. Apparently, in this case, the flake should conform to the peaks in the substrate but form a nanoscopic membrane on top of each valley, as was discussed in ref 13.

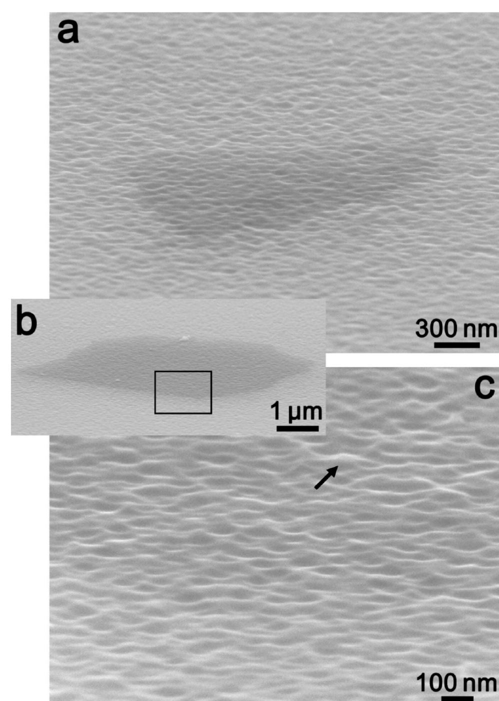

Figure 8. Side-view SEM images (tilt angle ~85°) of few-layer CCG flakes on Si/SiO_2 substrate. (a,b) SEM images of typical flakes. (c) High-magnification image of the area marked in (b) by the black rectangle. The arrow shows a rare wrinkle that is likely to be mostly caused by the rippling of the CCG flake rather than the underlying substrate.

The results of AFM analyses are in a good agreement with the side-view SEM images, although SEM is not a method routinely applied to the analysis of the nanoscopic corrugation of graphene materials. Figure 8 shows several SEM images of the GO flakes on the rough Si/SiO_2 substrate recorded at a very large tilt

angle (~85°). At such an angle, the roughness of the Si/SiO_2 substrate is clearly visible. Interestingly, similar roughness patterns can be observed for both the Si/SiO_2 surface and the GO flakes on the substrate, and only the brightness difference allows identification of the flakes (Figure 8a,b). Figure 8c shows a high-magnification image of a "borderline" between the flake and the empty substrate. These two areas appear exceedingly similar since the size of the peaks and valleys is on the order of a few tens of nanometers and their periodicity is similar for both areas; at the given brightness and contrast of the image, they are almost indistinguishable.

One may argue about the applicability of SEM to the analysis of corrugation of GO. However, it is known from TEM studies that the intrinsic rippling of the suspended graphene has an amplitude of about 1 nm and a coherence length of about 10 nm.[7] Clearly, in the bottom part of Figure 8c, one can see the roughness of the Si/SiO_2 substrate, which has similar amplitude and a coherence length of several tens of nanometers. If GO exhibited significant intrinsic corrugation in addition to the substrate-induced corrugation, the roughness pattern in the top part of Figure 8c would be different, with much smaller periodicity. However, with exception to a few wrinkles observed in these tilt-view SEM images, such as that shown by arrow in Figure 8c that could be attributed to GO, the majority of the Si/SiO_2 area covered with GO appears almost indistinguishable from the empty substrate. Therefore, such SEM images again suggest that GO flakes mostly conform to the substrate, and if other factors, such as intrinsic rippling of graphene, have an impact on the corrugation of GO, they demonstrate it on a smaller level, not observable by SEM.

In summary, we demonstrate that the corrugation of the monolayer CCG flakes and ribbons is mostly dictated by the roughness of the substrate. The effect of the substrate is so strong that even thermally induced contraction−expansion and removal of the oxygen-containing groups do not result in significant change in the corrugation of CCG. Our experimental observations are in accord with the results of our molecular dynamics simulations, which suggest that interaction with the substrate greatly suppresses the intrinsic corrugation of CCG. Since the substrate roughness is the predominant factor in determining the corrugation of surface-deposited CCG, using ultraflat substrates, such as freshly cleaved mica, allows preparation of flakes with a very low corrugation; the roughness of GO flakes on mica is ~70 pm. This is in accord with recent work,[33] which describes that ultraflat graphene can be obtained by deposition on the atomically flat terraces of cleaved mica surfaces. The reported height variation in the graphene layers observed by high-resolution AFM was less than 25 pm, less than reported in our work for GO flakes, indicating the suppression of any existing intrinsic ripples in graphene. Since SiO_2 is the most common surface upon which to fabricate graphene devices, in optimizing device embodiments, it is critical to recognize that the surface roughness, not the surface addends or thermal treatment, will dictate the graphene corrugation.

EXPERIMENTAL SECTION

For the simulations, we used the Forcite module of Accelrys Materials Studio 4.3 with Universal force field and atom-based electrostatic and van der Waals summation methods at the ultrafine level of quality. The molecular dynamics simulations were run with the starting temperature set at 298 K and NVE ensemble in 1 fs steps for 20 ps at a time (20 000 steps) divided in four equal consecutive runs of 5 ps each to manage operating system stability issues.

SEM analysis was performed using a JEOL-6500 field-emission scanning electron microscope. AFM images were obtained with a Digital Instruments Nanoscope IIIa, operating in tapping mode, using Si tips n-doped with 1−10 $\Omega \cdot$cm phosphorus (Veeco, MPP-11100-140) at a scan rate of 0.5 Hz and a resolution of 512 × 512. For the image analysis, we used the standard tools of the DI Nanoscope IIIa software. XPS analysis was performed with a PHI Quantera SXM scanning X-ray microprobe. Electronic devices were fabricated by standard electron beam lithography followed by electron beam evaporation of 20 nm thick Pt contacts. The electrical transport properties were tested using a probe station (Desert Cryogenics TT-probe 6 system) under vacuum with chamber base pressure below 10^{-5} Torr. The *IV* data were collected on an Agilent 4155C semiconductor parameter analyzer.

Acknowledgment. This work was supported by the Air Force Research Laboratory through University Technology Corporation, 09-S568-064-01-C1, the Air Force Office of Scientific Research FA9550-09-1-0581, the Army Research Office through an SBIR with Privatran LLC and the Office of Naval Research MURI Graphene Program.

REFERENCES AND NOTES

1. Novoselov, K. S.; Geim, A. K.; Morozov, S. V.; Jiang, D.; Zhang, Y.; Dubonos, S. V.; Grigorieva, I. V.; Firsov, A. A. Electric Field Effect in Atomically Thin Carbon Films. *Science* **2004**, *306*, 666–669.
2. Geim, A. K.; Novoselov, K. S. The Rise of Graphene. *Nat. Mater.* **2007**, *6*, 183–191.
3. Castro Neto, A. H.; Guinea, F.; Peres, N. M. R.; Novoselov, K. S.; Geim, A. K. The Electronic Properties of Graphene. *Rev. Mod. Phys.* **2009**, *81*, 109–162.
4. Geim, A. K. Graphene: Status and Prospects. *Science* **2009**, *324*, 1530–1534.
5. Peierls, R. E. Quelques Proprietes Typiques des Corpses Solides. *Ann. Inst. H. Poincare* **1935**, *5*, 177–222.
6. Landau, L. D. Zur Theorie der Phasenumwandlungen II. *Phys. Z. Sowjet Union* **1937**, *11*, 26–35.
7. Meyer, J. C.; Geim, A. K.; Katsnelson, M. I.; Novoselov, K. S.; Booth, T. J.; Roth, S. The Structure of Suspended Graphene Sheets. *Nature* **2007**, *446*, 60–63.
8. Meyer, J.; Geim, A.; Katsnelson, M.; Novoselov, K.; Obergfell, D.; Roth, S.; Girit, C.; Zettl, A. On the Roughness of Single- and Bi-Layer Graphene Membranes. *Solid State Commun.* **2007**, *143*, 101–109.
9. Bangert, U.; Gass, M. H.; Bleloch, A. L.; Nair, R. R.; Geim, A. K. Manifestation of Ripples in Free-Standing Graphene in Lattice Images Obtained in an Aberration-Corrected

Scanning Transmission Electron Microscope. *Phys. Status Solidi A* **2009**, *206*, 1117–1122.
10. Fasolino, A.; Los, J. H.; Katsnelson, M. I. Intrinsic Ripples in Graphene. *Nat. Mater.* **2007**, *6*, 858–861.
11. Ishigami, M.; Chen, J. H.; Cullen, W. G.; Fuhrer, M. S.; Williams, E. D. Atomic Structure of Graphene on SiO_2. *Nano Lett.* **2007**, *7*, 1643–1648.
12. Stolyarova, E.; Rim, K. T.; Ryu, S.; Maultzsch, J.; Kim, P.; Brus, L. E.; Heinz, T. F.; Hybertsen, M. S.; Flynn, G. W. High-Resolution Scanning Tunneling Microscopy Imaging of Mesoscopic Graphene Sheets on an Insulating Surface. *Proc. Natl Acad. Sci. U.S.A.* **2007**, *104*, 9209–9212.
13. Geringer, V.; Liebmann, M.; Echtermeyer, T.; Runte, S.; Schmidt, M.; Rückamp, R.; Lemme, M. C.; Morgenstern, M. Intrinsic and Extrinsic Corrugation of Monolayer Graphene Deposited on SiO_2. *Phys. Rev. Lett.* **2009**, *102*, 076102.
14. Morozov, S. V.; Novoselov, K. S.; Katsnelson, M. I.; Schedin, F.; Ponomarenko, L. A.; Jiang, D.; Geim, A. K. Strong Suppression of Weak Localization in Graphene. *Phys. Rev. Lett.* **2006**, *97*, 016801.
15. Katsnelson, M. I.; Geim, A. K. Electron Scattering on Microscopic Corrugations in Graphene. *Philos. Trans. R. Soc. London, Ser. A* **2008**, *366*, 195–204.
16. Lerf, A.; He, H.; Forster, M.; Klinowski, J. Structure of Graphite Oxide Revisited. *J. Phys. Chem. B* **1998**, *102*, 4477–4482.
17. Schniepp, H. C.; Li, J. L.; McAllister, M. J.; Sai, H.; Herrera-Alonso, M.; Adamson, D. H.; Prud'homme, R. K.; Car, R.; Saville, D. A.; Aksay, I. A. Functionalized Single Graphene Sheets Derived from Splitting Graphite Oxide. *J. Phys. Chem. B* **2006**, *110*, 8535–8539.
18. Stankovich, S.; Dikin, D. A.; Piner, R. D.; Kohlhaas, K. A.; Kleinhammes, A.; Jia, Y.; Wu, Y.; Nguyen, S. T.; Ruoff, R. S. Synthesis of Graphene-Based Nanosheets *via* Chemical Reduction of Exfoliated Graphite Oxide. *Carbon* **2007**, *45*, 1558–1565.
19. Gilje, S.; Han, S.; Wang, M.; Wang, K. L.; Kaner, R. B. A Chemical Route to Graphene for Device Applications. *Nano Lett.* **2007**, *7*, 3394–3398.
20. Gómez-Navarro, C.; Weitz, R. T.; Bittner, A. M.; Scolari, M.; Mews, A.; Burghard, M.; Kern, K. Electronic Transport Properties of Individual Chemically Reduced Graphene Oxide Sheets. *Nano Lett.* **2007**, *7*, 3499–3503.
21. Tung, V. C.; Allen, M. J.; Yang, Y.; Kaner, R. B. High-Throughput Solution Processing of Large-Scale Graphene. *Nat. Nanotechnol.* **2009**, *4*, 25–29.
22. Paci, J. T.; Belytschko, T.; Schatz, G. C. Computational Studies of the Structure, Behavior upon Heating, and Mechanical Properties of Graphite Oxide. *J. Phys. Chem. C* **2007**, *111*, 18099–18111.
23. Thompson-Flagg, R. C.; Moura, M. J. B.; Marder, M. Rippling of Graphene. *Europhys. Lett.* **2009**, *85*, 46002.
24. Gómez-Navarro, C.; Burghard, M.; Kern, K. Elastic Properties of Chemically Derived Single Graphene Sheets. *Nano Lett.* **2008**, *8*, 2045–2049.
25. Kosynkin, D. V.; Higginbotham, A. L.; Sinitskii, A.; Lomeda, J. R.; Dimiev, A.; Price, B. K.; Tour, J. M. Longitudinal Unzipping of Carbon Nanotubes To Form Graphene Nanoribbons. *Nature* **2009**, *458*, 872–876.
26. Hummers, W. S.; Offeman, R. E. Preparation of Graphitic Oxide. *J. Am. Chem. Soc.* **1958**, *80*, 1339.
27. Sinitskii, A.; Fursina, A. A.; Kosynkin, D. V.; Higginbotham, A. L.; Natelson, D.; Tour, J. M. Electronic Transport in Monolayer Graphene Nanoribbons Produced by Chemical Unzipping of Carbon Nanotubes. *Appl. Phys. Lett.* **2009**, *95*, 253108.
28. Higginbotham, A. L.; Kosynkin, D. V.; Sinitskii, A.; Sun, Z.; Tour, J. M. Lower-Defect Graphene Oxide Nanoribbons from Multiwalled Carbon Nanotubes. *ACS Nano* **2010**, *4*, 2059–2069.
29. Sinitskii, A.; Dimiev, A.; Corley, D. A.; Fursina, A. A.; Kosynkin, D. V.; Tour, J. M. Kinetics of Diazonium Functionalization of Chemically Converted Graphene Nanoribbons. *ACS Nano* **2010**, *4*, 1949–1954.
30. The schematic in Figure 3a does not imply that the ribbons necessarily have armchair edges. In fact, according to the proposed mechanism of unzipping (see refs 25, 28, and 31), the ribbons most likely have zigzag edges, though this fact still requires experimental verification.
31. Rangel, N. L.; Sotelo, J. C.; Seminario, J. M. Mechanism of Carbon Nanotubes Unzipping into Graphene Ribbons. *J. Chem. Phys.* **2009**, *131*, 031105.
32. Bao, W.; Miao, F.; Chen, Z.; Zhang, H.; Jang, W.; Dames, C.; Lau, C. N. Controlled Ripple Texturing of Suspended Graphene and Ultrathin Graphite Membranes. *Nat. Nanotechnol.* **2009**, *4*, 562–566.
33. Lui, C. H.; Liu, L.; Mak, K. F.; Flynn, G. W.; Heinz, T. F. Ultraflat Graphene. *Nature* **2009**, *462*, 339–341.